energies

MDPI

Article

Cooling Thermal Comfort and Efficiency Parameters of Ceiling Panels, Underfloor Cooling, Fan-Assisted Radiators, and Fan Coil

Karl-Villem Võsa [1,2,*], Andrea Ferrantelli [1,2,3] and Jarek Kurnitski [1,2,3]

1 FinEst Centre for Smart Cities (Finest Centre), Tallinn University of Technology, 19086 Tallinn, Estonia; andrea.ferrantelli@taltech.ee (A.F.); jarek.kurnitski@taltech.ee (J.K.)
2 Nearly Zero Energy Buildings Research Group, Tallinn University of Technology, 19086 Tallinn, Estonia
3 Department of Civil Engineering, Aalto University, FI-02150 Espoo, Finland
* Correspondence: karl-villem.vosa@taltech.ee

Abstract: Climate change has brought a compelling need for cooling living spaces to the attention of researchers as well as construction professionals. The problem of overheating enclosures is now exacerbated in traditionally affected areas and is also affecting countries that were previously less prone to the issue. In this paper, we address measurements of thermal comfort and cooling emission efficiency parameters for different devices: ceiling panels, underfloor cooling, fan-assisted radiators, and fan coil. These devices were tested in low and high cooling capacities of up to 40 W/m^2 while also featuring heating dummies to imitate internal heat gains. Air temperatures were measured at different heights, allowing to evaluate the thermal stratification with high accuracy. Thermal comfort differences of the tested systems were quantified by measuring both air velocities and operative temperatures at points of occupancy. In summary, the best-performing cooling devices for the studied cooling applications were the ceiling panels and fan radiators, followed by underfloor cooling, with a limitation of stratification. Because of the strong jet, fan coil units did not achieve thermal comfort within the whole occupied zone. The results can be utilized in future studies for cooling emission efficiency and energy consumption analyses of the different cooling devices.

Keywords: cooling; measurements; ceiling panels; underfloor cooling; fan-assisted radiators; fan coil; energy efficiency

check for updates

Citation: Võsa, K.-V.; Ferrantelli, A.; Kurnitski, J. Cooling Thermal Comfort and Efficiency Parameters of Ceiling Panels, Underfloor Cooling, Fan-Assisted Radiators, and Fan Coil. *Energies* **2022**, *15*, 4156. https://doi.org/10.3390/en15114156

Academic Editor: Dmitry Eskin

Received: 20 May 2022
Accepted: 4 June 2022
Published: 5 June 2022

Publisher's Note: MDPI stays neutral with regard to jurisdictional claims in published maps and institutional affiliations.

Copyright: © 2022 by the authors. Licensee MDPI, Basel, Switzerland. This article is an open access article distributed under the terms and conditions of the Creative Commons Attribution (CC BY) license (https://creativecommons.org/licenses/by/4.0/).

1. Introduction

In view of the multifaceted challenge provided by the climate change, with more frequent, intense, and longer-lasting heat waves [1], the technology of current HVAC (heating, ventilation and air conditioning) systems needs to be updated towards an improved resilience of their operation and reduced emissions [2]. A target of restricting the median warming to 1.5 °C by the year 2100 has been set by global regulations [3]; furthermore, it has been shown that the increasing trends in cooling energy demand in the last 30 years are more pronounced than the decreasing trends in heating [4]. This happens due to a high correlation between overheating living spaces and worsening health conditions of the occupants [5].

Investigating new technologies and HVAC design methods for the optimization of cooling systems towards energy efficiency, emissions reduction, and thermal comfort is therefore of the outmost importance in the current climate emergency.

The European Standard EN 15316-2 [6] evaluates the efficiency of space emission systems as a sum of different cooling set-point offsets; these reflect any system inefficiencies regarding distribution, control, and emissions. Such a shifted set-point temperature is then used to compute the annual cooling energy demand by means of a discrete set of default values that are provided in the standard. Product-specific values or different tabulated

values from national annexes can be used as well; however, the specific methods for their measurements and derivations of these parameters are not fully specified.

This paper tackles this issue by providing experimental evidence for a two-fold task: (i) comparing several different cooling devices to support the design of HVAC strategies and (ii) developing analytical/numerical methods for computing the values that are used in the annual cooling energy demand estimations.

Specifically, our measurements address four devices: radiant ceiling cooling panels (RCCPs), fan-assisted radiators, underfloor cooling, and fan coil units (FCUs). Traditionally, the focus of the vast majority of investigations has been on heating rather than on cooling; even comprehensive reviews of the actual research status typically address cooling and heating (see [7] and references quoted therein). Whether and in what measure the radiant systems are better-performing than convective systems is not yet established [8].

Ceiling radiant cooling panels (CRCPs) are widely investigated due to the various applications in both heating and cooling together with technical design perspectives on many aspects. A large number of studies exists, addressing simulations [9] as well as experimental assessments: the cooling capacity and energy performance of CRCP systems can be improved in many different ways. An open-type CRCP system with air circulators provided a maximum increment of 26.2% in cooling capacity [10], while segmented and concave surfaces provided an improvement in energy performance relatively to flat panels [11]. The interaction of ceiling panels with changing boundary conditions within the room was investigated in [12].

Panel radiators have been subject to performance testing not only for heating but also for cooling for decades, with earlier studies focusing on both experimental [13] and modelling aspects [14]. However, the interest has always been overwhelmingly in favor of heating; the fan-assisted design is also less commonly addressed although it has been experimentally proven to be very effective for cooling (see e.g., [15]).

Underfloor cooling has been the object of intense research due to the structural similarity and operation with underfloor heating [16] but also due to condensation risk and low cooling capacity [17]; moisture condensation at the floor surface is usually avoided by supplying conditioned dry air within ventilation ducts [18]. All in all, research papers on this topic are quite numerous, ranging from the implementation of phase-change materials (PCM) into the system design [19] to thorough testing of the heat-transfer process occurring over the floor surface [20].

Fan coil units (FCU) probably constitute the most traditional active cooling system; however, they are still widely adopted and constantly investigated due to their performance and variety of applications. These convective devices have proven to be a valid cooling solution until today and are even capable of outperforming radiative devices [21], both concerning indoor temperature uniformity as well as energy performance [22]. The authors of [23] also found no significant difference between convective and radiant heating systems regarding thermal sensation. Unfortunately, problems with thermal comfort at higher cooling loads do exist with this system, mostly due to high air-flow rates being needed, which yield high velocities into occupied zones from the devices. This typically causes draught and is not pleasant for the occupant [24].

Despite all these in-depth individual investigations, it is hard to find systematic analyses covering a wide choice of different systems. For instance, several studies about implementation of cooling devices for personal usage, such as the so-called personal comfort systems (PCS), have investigated their energy-saving potential in regards to usage behaviors [25,26]. However, a direct comparison between PCS devices is prevented by various experimental conditions such as temperature differences and clothing insulation [27].

Radiant ceiling panels were compared to a fan-coil unit in [28], which measured a more resilient and performing operation for the radiative (ceiling panel) compared to the convective unit (FCU). They also obtained a 14% decrease in pump energy use when using an operative temperature sensor to provide a feedback signal to the control system.

Interestingly, this was one of the few studies to address the operative temperature, which is still rather overlooked.

In other words, although there exists a wide research and technical literature describing each single apparatus, comprehensive studies that indicate how these four cooling systems compare to each other under the same operating conditions cannot be found yet. The role of the operative temperature on thermal comfort has also been overlooked quite systematically. No studies indicating the parameter values that are needed to calculate the temperature deviation setpoints are present either, leaving the calculation of annual cooling energy demand to default values reported in the standards.

In this paper, we contribute to filling this research gap by means of a thorough experimental comparison of the cooling efficiency of four devices, both radiative and convective. After discussing each of them in detail as well as the overall methodology and measuring setup in Section 2, Section 3 reports vertical thermal gradients, operative temperatures, air velocities, surface temperatures, and the results of smoke visualizations. Our results are discussed in Section 4, and conclusions are drawn in Section 5.

2. Materials and Methods

An office-like situation with six desks was created in the testing facility, where heating dummies were used to imitate the thermal output from humans, and an additional cooling load was created with convective electric radiators. Temperature sensors were configured to collect data every 10 s. The study first considered the power output of four different cooling systems; afterwards, we addressed the effect of air movement that was generated by the systems on the indoor climate, including a visualization through smoke tests.

2.1. nZEB Test Facility at TalTech and General Setup

The cooling devices were tested at the nZEB test facility in the Tallinn University of Technology campus [29], which is pictured in Figure 1. Four different cooling devices were installed in a 30 m^2 seminar/classroom located on the east side of the building, featuring four windows: one on each north and south facades and two on the east-facing external wall. This test room has a false ceiling, while the whole facility has a suspended floor with a ventilated crawlspace.

Figure 1. The TalTech nZEB experimental facility [30].

Chilled water for the cooling systems is produced on-site with an air-to-water heat pump, with an additional free cooling circuit available with a separate plate heat exchanger and dry cooler when ambient temperature is sufficiently low. Both produce chilled water into an accumulation tank. In the building, there is a built-in mixing unit that allows supply water to be mixed at the required temperature in the secondary system while measuring both primary and secondary temperatures upstream and downstream. The mixing station is also equipped with an ultrasonic volume flow meter to measure the secondary flow and enables the calculation of the cooling capacity.

The operating principle of the hydraulic installation is shown in Figure 2**.** Air-to-water heat pump operated at a single compressor speed and produced chilled water with a set-point temperature of +10 °C to the buffer tank. A hysteresis of ±2 °C was set to ensure that a sufficiently low temperature was delivered to the mixing valve.

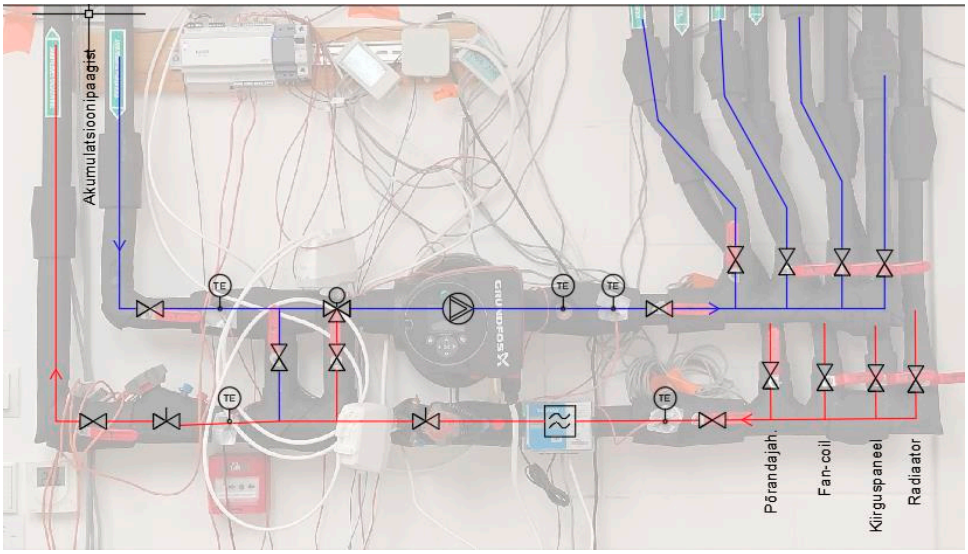

Figure 2. Mixing unit connections: underfloor, fan-coil, cooling panels, radiator (left to right).

The supply temperature to the cooling devices was controlled by a three-way mixing valve with 3 mm travel, which was operated with a TA Slider 160 actuator. The input signal of the actuator was generated by a temperature control loop that was implemented in Python (simple-PID library) according to Equation (1), with chosen controller parameters K_p = 1800, K_i = 60, and K_d = 13,500,

$$u(t) = K_p e(t) + K_i \int_0^t e(\tau) d\tau + K_d \frac{de(t)}{dt}. \quad (1)$$

Additionally, a balancing valve TA STAD-15 was installed on the return of the secondary loop to confirm the flow-rate values to the devices. However, due to the low flow measurement accuracy (≥4%) from the differential pressure over the balancing valve, for measuring the volumetric flow rate in the secondary loop, we used a separate ultrasonic flow meter.

The test facility is equipped with mechanical heat recovery ventilation capable of a maximum air exchange of 550 m^3/h. Ventilation flow rates were set in this study to ensure a constant air circulation of value 45 L/s (or 1.5 L/m^2) in the tested room following the recommendation of [31] to ensure good air quality. Supply air was pre-heated, and measured temperatures varied between 19 °C and 21 °C.

2.2. Measurement Equipment

A total of 28 temperature sensors were installed in the building for measuring various air and surface temperatures inside the tested room as well as air temperatures of the bounding rooms (two testing rooms, corridor, toilet) behind the false ceiling and in the crawlspace. Five more sensors were installed in the mixing unit measuring point and another one in the flow measuring point. Measuring the temperatures in the mixing unit allowed to calculate the cooling capacity of the different systems by using the following Equation (2):

$$\phi = G \times c \times \rho \times \Delta t, \quad (2)$$

where ϕ is the cooling capacity (W), G is the water flow (m^3/s), c is the specific heat capacity of the water (J/(kg°C)), ρ is the water density (kg/m^3), and Δt is the difference between the flow and return water temperatures (°C).

In the case of cooling radiators, four measuring points were installed directly on the device. Three sensors were placed on the front panel surface at heights of 50, 300, and 550 mm to map the temperature distribution on its surface. One measuring point was above the radiator at 20 mm from the top grille to measure the temperature of the air that was blown out by the fans.

Four additional sensors were installed on the ceiling panels. Two measuring points were installed at the center of both panels to measure the difference in surface temperatures of the panels. A third one was installed at 100 mm below the center of the first panel to characterize the air temperature near the panel. The fourth sensor was located between the first panel and the ceiling at 10 cm below the ceiling.

For floor cooling, we installed six surface temperature sensors, two of which were located on one third of the side of the room, to characterize the overall floor surface temperature. The other two measuring points were installed in the inlet pipe of the floor circuit, and the last two in the return circuits. They measured the heating of the coolant, which leads to a change in the floor surface temperatures. Two sensors were installed behind the plafond: one for the inflow and the other for the outflow.

For all systems, the gradients and air flow speeds were measured by five dedicated thermo-anemometers along with operative temperature and relative humidity sensors that were installed on the same tripod (Figure 3a). The operative temperature was recorded at the heights of 0.1, 0.6, 1.1, 1.7, and 2.9 m. A FLIR E95 thermal camera captured the temperature distribution from the thermal images of each cooling device; using a fog generator also allowed visualizing the air distribution of the four cooling systems. The ventilation air-flow rates were set by means of a capture hood and a differential pressure manometer with valve position measurement. The characteristics of the sensors employed in this study are reported in Table 1, where the bold text identifies different sensor types.

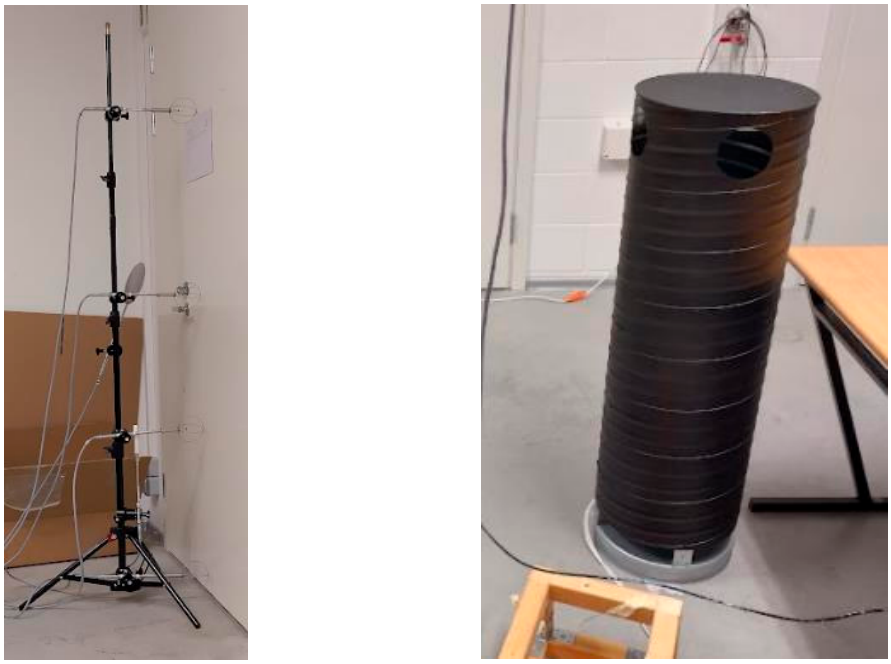

(**a**) (**b**)

Figure 3. Measuring tripod (**a**) and heating dummy (**b**).

Table 1. Characteristics of the sensors employed in the experiments.

Mixing Station Sensors	Meas. Range	Accuracy
Fluid temperature	−50 . . . +250 °C	±0.15 + 0.002 | t | °C
Air temperature	−40 . . . +50 °C	±0.15 °C
Surface temperature	−40 . . . +50 °C	±0.15 °C
Flow meter	0 . . . 3.125 m^3/h	±3%
Room/device sensors		
Thermo-anemometer	0.05 . . . 5.00 m/s	±0.02 m/s
	−20 . . . +80 °C	±0.20 °C
Operative temperature	0 . . . +45 °C	±0.20 °C
Relative humidity	0 . . . 100%	±1.50%

Six heating dummies as seen in Figure 3b were used. These feature three incandescent lamps, which, according to the EN 14240 Standard [32], provide a total rated output of 3 × 60 W per dummy. To provide a sufficient cooling load, two electric radiators with rated heat output of 1000 W were additionally used. Figure 4b illustrates the positioning of dummies and radiators; that of sensors is given in Figure 5a, and the vertical positioning of the sensors is provided in Figure 5b.

(**a**) (**b**)

Figure 4. Tripod setup (**a**) for measuring the thermal comfort and (**b**) positioning of heating dummies (circles) and measuring tripod (cross).

2.3. Thermal Comfort

Air stratification and vertical temperature distribution were computed according to two different procedures in the EN16798-1 standard. The vertical air temperature difference γ_1 (head-ankle) [33] and the total ceiling-floor gradient γ_{TOT} are determined as follows:

$$\gamma_1 = t_{1.1} - t_{0.1} \quad (3)$$

$$\gamma_{TOT} = t_{2.9} - t_{0.1} \quad (4)$$

with t_z the air temperature at height z (m). The operative temperature probe was installed at h = 1.10 m, and it was displaced by 30° from the vertical. Comparing this value to the air

temperature at the same height allowed to assess whether a higher room air temperature can be allowed while keeping the same sensed temperature of the occupant. Velocity data from the thermo-anemometers were logged and analyzed from the tripod setup as well. The setup is pictured in Figure 4a.

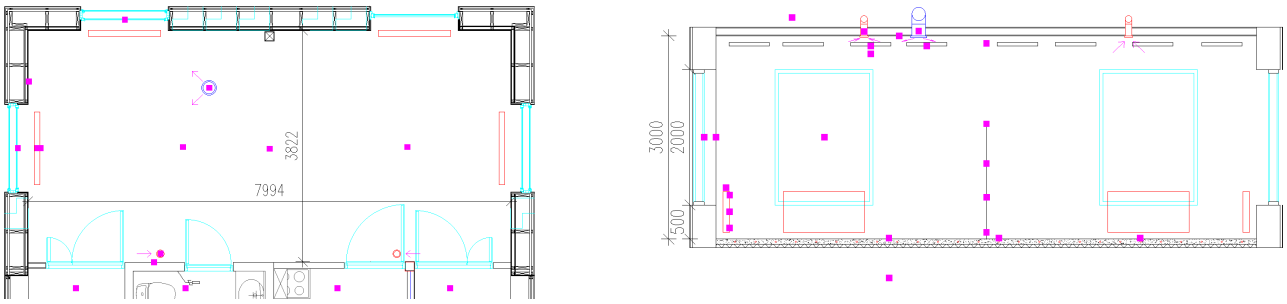

(**a**) (**b**)

Figure 5. Plan view of installed sensors (**a**); vertical section of the installed sensors (**b**).

2.4. Ceiling Panels

Eight ceiling panels in total, with dimensions 600 × 3000 mm, were installed using suspension cables at a height of 2.85 m, namely at 0.15 m from the ceiling. The side facing the ceiling was insulated with mineral wool insulation plates that were provided by the manufacturer. The ceiling panels were arranged into four pairs, where the two panels were connected in series. Nominal conditions and cooling output for a serially connected pair are reported in Table 2.

Table 2. Nominal operation parameters of a ceiling panels pair.

Parameter	Value
Supply temperature, °C	15.0
Return temperature, °C	19.0
Room air temperature, °C	25.0
Volume flow, l/h	76.3
Pressure loss, kPa	13.2
Cooling output per pair, W	354.7

Finally, a visual of the panels' layout is given in Figure 6 below.

Figure 6. Installation of the ceiling panels.

2.5. Fan-Assisted Radiator

Four 22-type radiators (two panels with two convective fins) with steel panels measuring 600 × 1200 mm were installed under the test room windows. On top of the radiator, under the cover grille, an array of fans is installed for enhancing the cooling output of the radiator. These fans displace air upwards into the room to prevent a cold down-draught to the floor, while the temperature difference between the air entering the channel and

the cooling panel surface controls the fan speed. The radiators' specifications are listed in Table 3, and pictures of the fans array and an overall view of the device are given in Figure 7.

Table 3. Nominal operation parameters of the panel radiators.

Parameter	Value
Supply temperature, °C	15.0
Return temperature, °C	17.5
Room air temperature, °C	28.1
Volume flow, l/h	131.8
Cooling output, W	390.0

(**a**) (**b**)

Figure 7. Array of the fans with removed covering grill (**a**) and view of the radiator (**b**).

2.6. Underfloor Cooling

Existing underfloor heating loops were used for testing the underfloor cooling. For switching to the cooling circuit, supply and return lines before the manifold were retrofitted with three-way and isolating ball valves. Pe-PEX pipes of dimensions 20 × 2.0 mm were installed in a 40 mm screed layer with a 300 mm pipe spacing. The resulting cooling output was estimated to be 750 W (25 W/m^2) at operating conditions (14.0/17.0/26.0 °C supply/return/room air temperature). Figure 8 features both a thermographic image of the piping as well as its overall arrangement in the nZEB testing facility.

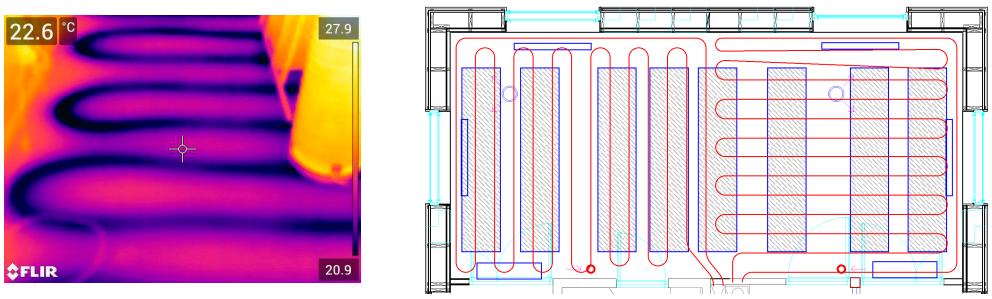

(**a**) (**b**)

Figure 8. Thermographic image of the underfloor piping (**a**) and piping positioning layout (**b**).

2.7. Fan Coil Unit

We used two existing FCUs, which were mounted on the wall, with nominal cooling capacity and operating conditions at the lowest fan speed as reported in Table 4. During the measurements, the FCUs were operated at this lowest fan speed.

Table 4. Nominal operation parameters for the fan coil unit (FCU).

Parameter	Value
Supply temperature, °C	7
Return temperature, °C	12
Room air temperature, °C	27
Air volume flow, m^3/h	390
Volume flow, L/h	511
Pressure loss, kPa	35.6
Cooling output, W	2120

3. Results

A summary of hourly averaged values of cooling outputs and hydraulic data for each measurement is given in Table 5.

Table 5. Test conditions, 1-hour values.

System	Supply Temperature, °C	Return Temperature, °C	Room Air Temperature, °C	Chilled Water Flow Rate, l/h	Cooling Power, W	Cooling Power, W/m^2
Ceiling panels HIGH	15.09	17.96	25.38	335	1128	36.7
Ceiling panels LOW	18.50	20.60	26.66	337	820	26.7
Fan-assisted radiator HIGH	15.00	17.70	24.98	338	1061	34.6
Fan-assisted radiator LOW	15.25	17.41	25.14	345	869	28.3
Underfloor cooling	15.00	17.19	25.84	328	836	27.2
Fan coil units	17.00	21.00	25.88	334	1552	50.6

3.1. Thermal Gradients within the Room

The highest temperature gradient was generated by the underfloor cooling system with γ_1 = 2.93 °C/m and γ_{TOT} = 1.51 °C/m, as illustrated in Figure 9a. This is expected since no buoyancy-induced mixing can be generated within the room, as the cooled air mass close to the floor is denser than the air layers above. Conversely, the fan coil unit generated almost no temperature gradient in the occupied zone. Only some temperature rise occurred at h = 2.90 m, giving γ_1 = 0.14 °C/m and γ_{TOT} = 0.57 °C/m, as plotted in Figure 9b.

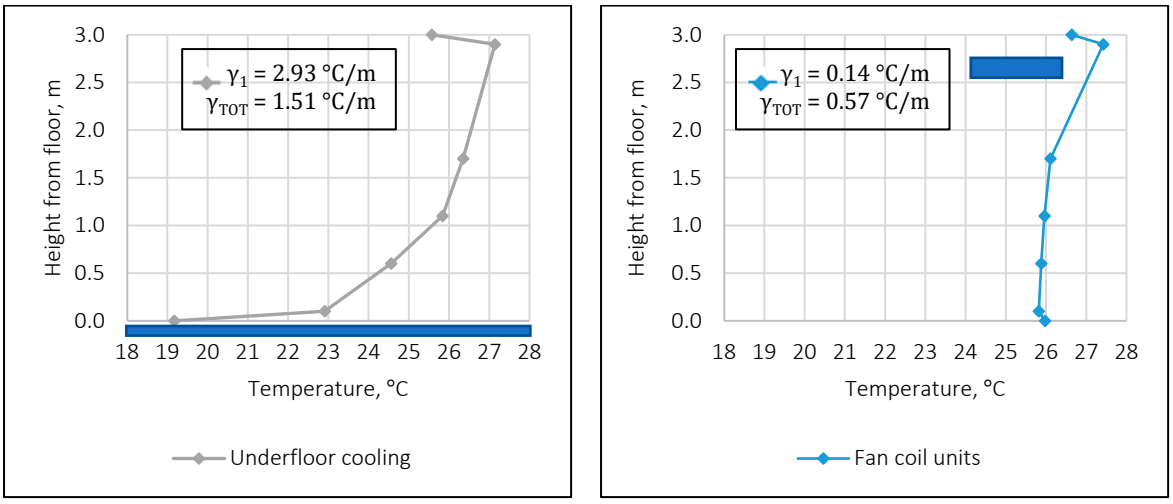

(**a**) (**b**)

Figure 9. Measured temperature gradient of underfloor cooling (**a**) and fan coil unit (**b**).

Virtually no stratification in the occupied zone was detected with cooling panels and radiators at the higher cooling output, as pictured in Figure 10. At the lower cooling output, there exists some stratification, with γ_1 = 1.35 °C/m for ceiling panels and γ_2 = 0.97 °C/m for radiators.

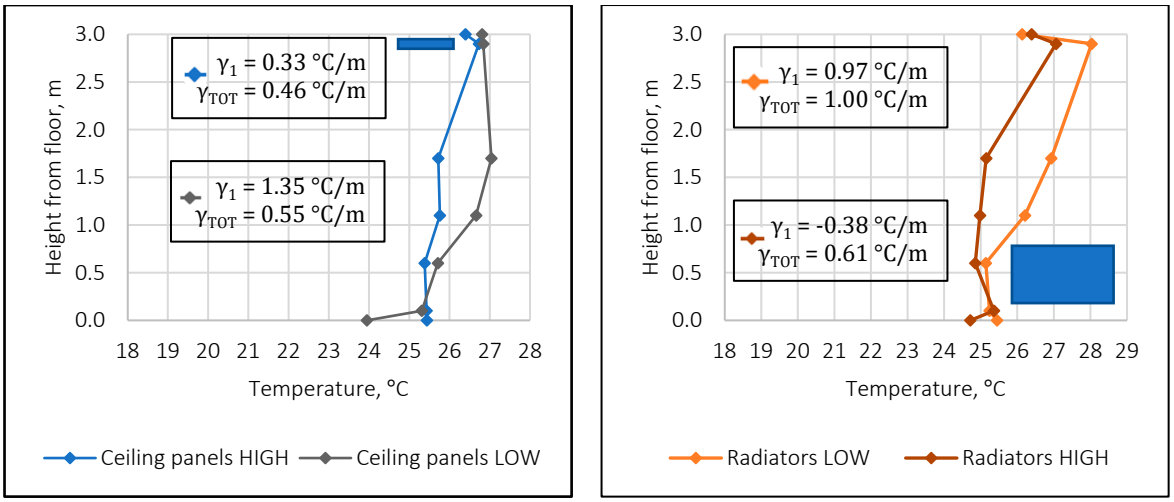

(**a**) (**b**)

Figure 10. Measured temperature gradient of ceiling panels (**a**) and panel radiators (**b**).

3.2. Operative Temperature

Figure 11 portrays the measured difference between operative and air temperatures. This is overall quite substantial; a greater surface area (ceiling panels and underfloor cooling) is correlated with a larger difference, which can be as high as −1.28 °C for ceiling panels measured at the lower cooling output. On the other hand, the opposite effect holds for the FCUs that provides $t_{op} - t_{1.1}$ = 0.27 °C.

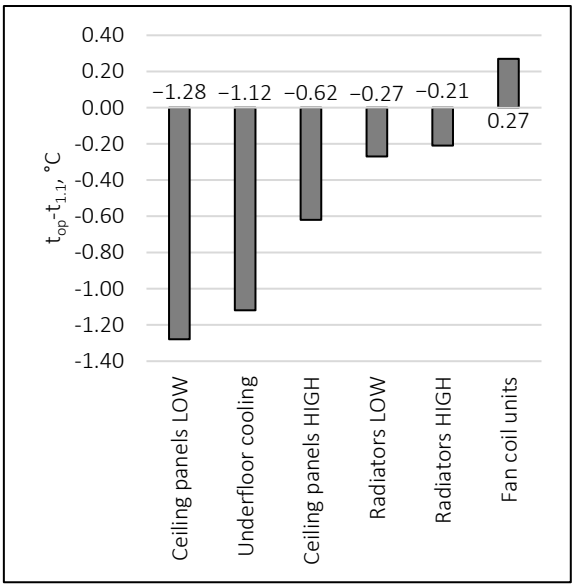

Figure 11. Measured difference between operative and air temperature.

For both ceiling panels and underfloor cooling, the lower cooling outputs have a higher temperature differential because the higher radiant heat exchange to the colder surface is offset by the lower temperature gradient.

3.3. Air Velocity Magnitudes

Measurements of the air velocity magnitude from the thermal comfort tripod are reported in Table 6, showing a clear consistency with the thermal stratification results plotted in Figures 9 and 10: higher velocities lead to higher mixing of air and vice versa.

Table 6. Air velocities as measured on the tripod. Cat. I in green, Cat. II in yellow, Cat. III in orange, and the exceeding thermal comfort class boundaries are in red.

Height/ System	Ceiling Panels HIGH, m/s	Ceiling Panels LOW, m/s	Radiators HIGH, m/s	Radiators LOW, m/s	Underfloor Cooling, m/s	Fan Coil Units, m/s
2.90 m						
1.70 m						
1.10 m						
0.60 m						
0.10 m						
2.90 m	0.19	0.06	0.11	0.19	0.08	0.19
1.70 m	0.07	0.26	0.08	0.07	0.02	0.88
1.10 m	0.04	0.13	0.12	0.04	0.02	0.45
0.60 m	0.10	0.03	0.09	0.10	0.02	0.25
0.10 m	0.03	0.03	0.06	0.03	0.02	0.61

Regarding the FCU system, the air velocities in the occupied zone for both a seated and standing occupant are in class IV [33]. No significant differences of air velocities along the height of the room in the measurement point were detected. The air velocities for the underfloor cooling are minimal, averaging at 0.02 m/s for both a seated and standing occupant, while higher air velocities in the radiator HIGH tests compared to the radiator LOW tests were observed.

Ceiling panel tests exhibited a rather different behavior when comparing the HIGH and LOW outputs, as the LOW output air velocities approached 0.26 m/s at h = 1.70 m. One would expect that if the higher cooling output achieved Cat. I in thermal comfort, the same would hold true for the lower cooling power as well, but it is possible that either the ventilation supply jet or thermal plumes initiated by internal heat gains started to dominate at this lower cooling output. At the most critical height of 1.1 m, the velocities were low at both cooling outputs.

3.4. Thermal Imagery and Measured Surface Temperatures

The thermal images of the cooling devices' surfaces are depicted in Figures 12 and 13. The visualized temperatures assume a surface emissivity $\varepsilon = 0.95$.

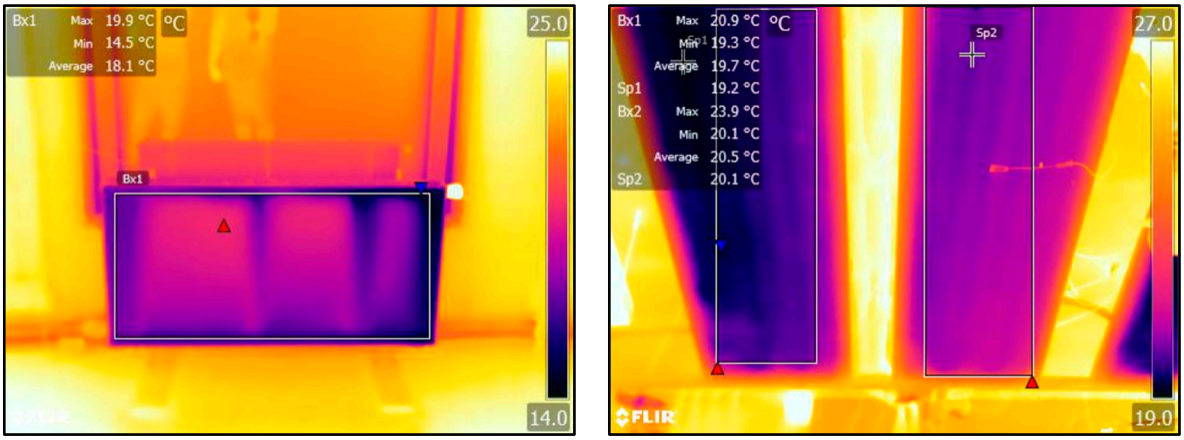

(**a**) (**b**)

Figure 12. Thermal image of radiator HIGH (**a**) and of ceiling panels LOW (**b**).

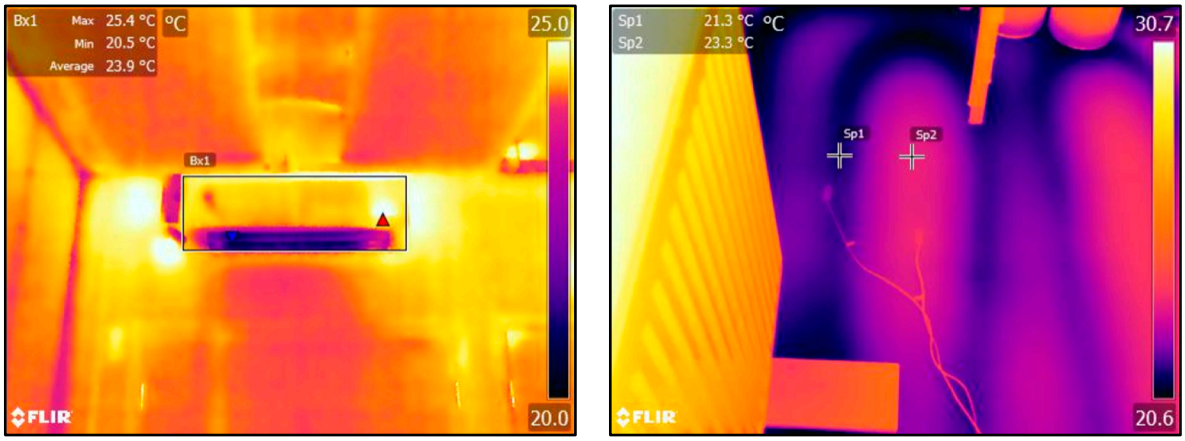

(**a**) (**b**)

Figure 13. Thermal image of the FCU (**a**) and of the underfloor cooling (**b**).

The temperature distribution induced by the fans drawing air through the radiator's panels is very evident in Figure 12a. The perimeter of the radiator is cooler, consistent with a lower convective heat transfer due to lower air velocities.

Figure 12b reports the thermal image of a serially connected pair of cooling panels. The one on the left has lower surface temperatures (it is connected directly to the supply line of the chilled-water loop), while the supply of the panel on the right is connected to the return line of the panel on the left. Our measurements showed an average 1.0 °C surface temperature difference between the two panels.

In Figure 13a, we portray the cooling coil of the FCU. As this is mostly relying on convection, the negligible surface area and solid angle between the occupant and the coil are uninfluential to the radiative heat transfer and its effect on the operative temperature. A section of the underfloor cooling system is instead shown in Figure 13b: a 2.0 °C temperature difference was observed both on top of the pipe (Sp1) and between pipes (Sp2).

Additionally, surface temperatures at different locations were measured with sensors; these are reported in Table 7.

Table 7. Surface temperatures as measured with sensors.

Device	Sensor	Temp., °C
Ceiling panels HIGH	1st in series	16.30
	2nd in series	17.75
Ceiling panels LOW	1st in series	19.36
	2nd in series	20.38
Radiators HIGH	h = 0.05 m	17.88
	h = 0.30 m	18.61
	h = 0.55 m	-
Radiators LOW	h = 0.05 m	17.37
	h = 0.30 m	19.02
	h = 0.55 m	19.41
Underfloor cooling	On supply pipe	17.85
	b/w supply pipes	19.03
	On return pipe	19.65
	b/w return pipes	20.37

3.5. Smoke Visualisation Experiments

For visualizing the air distribution patterns around the cooling systems (except for the underfloor cooling), we used a fog machine. Such visualization is matched with velocity measurements to assess a possible thermal discomfort in the occupied zone both qualitatively and quantitatively.

The dissipation of the fog for the HIGH case of ceiling panels is pictured in Figure 14. Compared to the LOW case (not shown as the visual effect was not evident from pictures), we observed a quicker detachment from the ceiling and cooling panels towards the room due to a higher buoyancy induced by lower surface temperatures. The fog reached the mid-height of the room in 15 s at a low velocity.

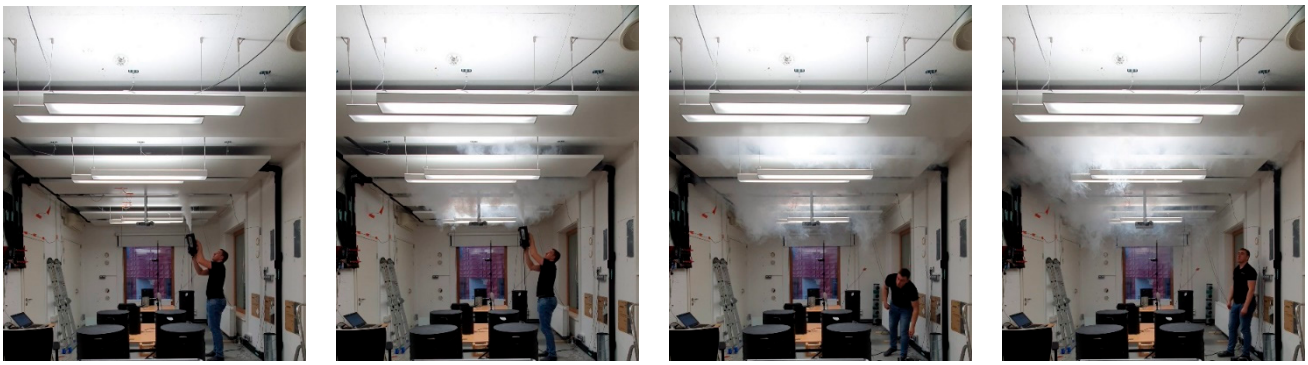

Figure 14. Air circulation pattern of ceiling panels HIGH. Periodic snapshots every 5 s.

Figure 15 shows the jet from the FCU fan. The air speed is always relatively high even at lowest fan speed settings, reaching the floor of the room in 5 s. Further dissipation of the fog was observed along the floor of the room as well.

Figure 15. Air circulation pattern of FCUs. Periodic snapshots every 5 s.

Finally, the effects of both LOW and HIGH radiator settings are, respectively, shown in Figures 16 and 17. To supply and distribute the fog to the bottom of the radiator, we used a duct with five tee fittings; some individual jets from the fan arrays are visible in the first image. There is a clear distinction in the results: as in the HIGH configuration the fan speed was at maximum, the fog easily reached the ceiling; for the LOW case, the cooled air could reach only a height of ~2.00 m before developing towards the room.

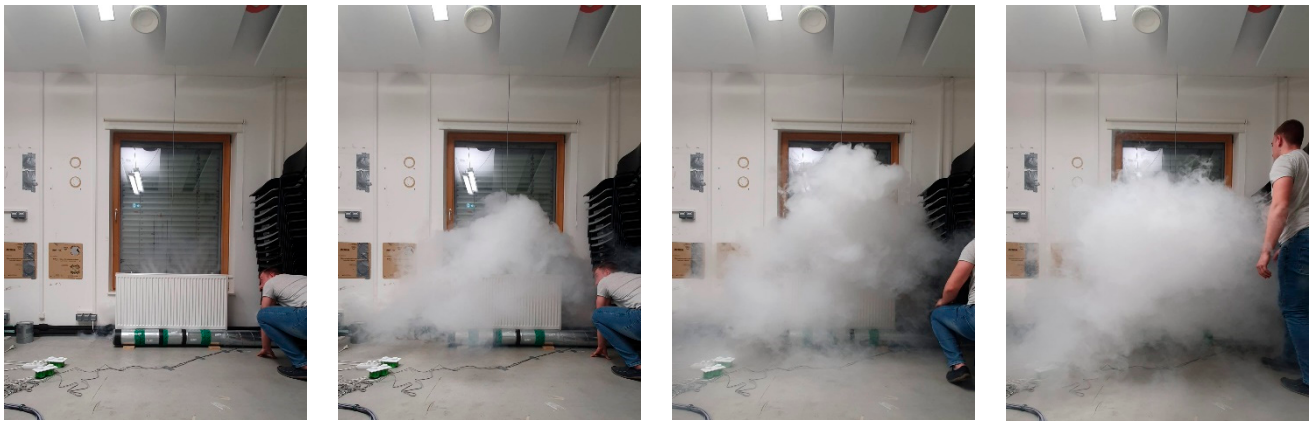

Figure 16. Air circulation pattern of radiators LOW. Periodic snapshots every 5 s.

Figure 17. Air circulation pattern of radiators HIGH. Periodic snapshots every 5 s.

It is worth noting that the supply valve above the radiator in Figure 16 might have somewhat suppressed the upward plume for the LOW case. The situation is schematized in the air velocities reported in Figures 18 and 19. The same approach was repeated to obtain Figure 20 for the fan coil unit.

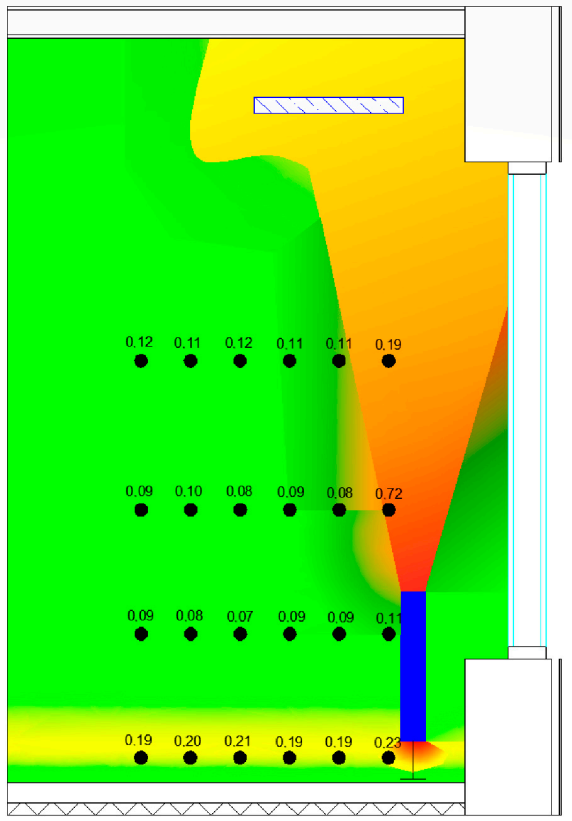

Figure 18. Air jet velocities for cooling radiators, HIGH speed.

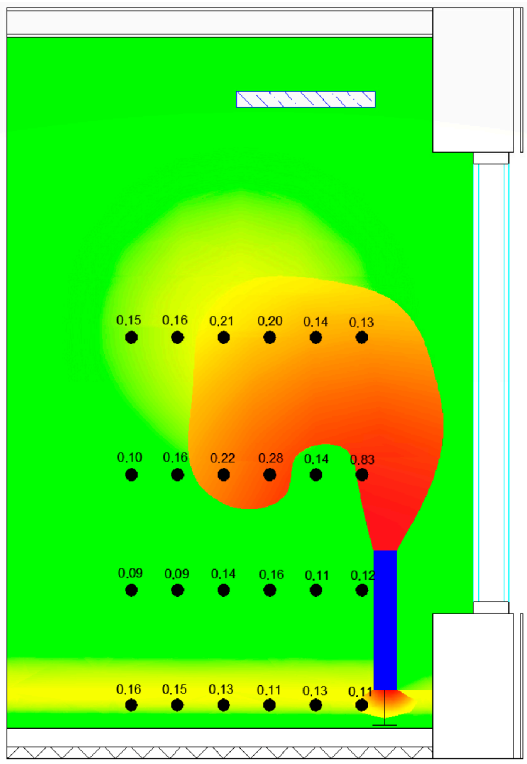

Figure 19. Air jet velocities for cooling radiators, LOW speed.

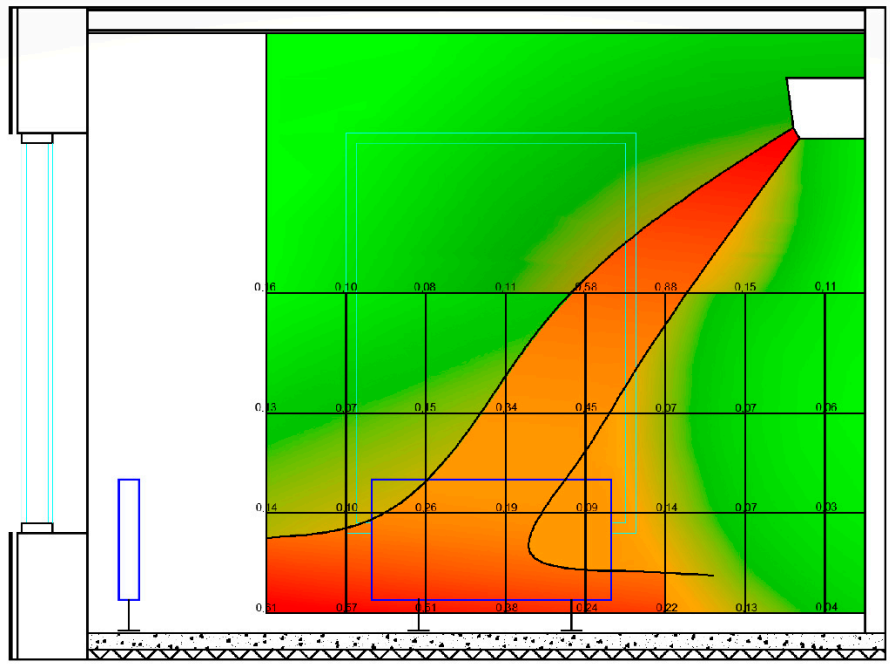

Figure 20. Visualization of the air jet velocities for the FCU unit.

4. Discussion

Considering the whole set of cooling devices, the vertical thermal stratification in the room showed a clear difference between the underfloor cooling system and the other devices. A substantial thermal gradient, i.e., 2.93 °C for a seated occupant (head to ankle), was generated via buoyancy effects (Figure 9) by the underfloor cooling, which, at the measured cooling outputs, was the only system providing a comfort class II (EN 16798-1 standard [33]). Importantly, such temperature difference is also influenced by the vertical temperature distribution, thus requiring a simultaneous assessment in terms of energy efficiency. The air speed measurements in Table 6 show very clearly that the underfloor cooling provided minimal circulation, with average values of 0.02 m/s for both a seated and standing occupant, while higher air velocities were observed in the radiator HIGH tests compared to those for the radiator LOW. Although this is expected due to the maximum fan speed output, in the HIGH case, the measured air velocities were still low enough to stay within the first category of thermal comfort. The underwhelming FCU performance is instead critically affected by jet direction and sensors positioning; when during the testing, the measurement point was located away from the device, class II was reached. On the other hand, when evaluated within the entire occupied zone according to EN 16798-1:2019, the FCU drops to class IV. Therefore, whilst inducing some excellent buoyancy-driven mixing, the high air velocities are unacceptable for thermal comfort and require no occupancy under the air jet.

The radiation panel and the fan radiator operating at higher cooling capacity/higher fan speed (HIGH) provided an operative temperature that was lower than the air temperature, see Figure 11. Both underfloor cooling and LOW-speed radiator achieved operative temperatures that were higher by, respectively, 0.2 °C and 0.1 °C. Finally, the FCU showed that although the room air temperatures varied over a very small range, the operative temperature was always higher.

The smoke tests proved to be very useful for visualizing the air distribution patterns around the cooling systems. Figures 16 and 17 portray very clearly the radical effect of the fan in the case of radiators. This is also quantified in Figure 19, where the smoke is confirmed to reach only a height of 2 m before collapsing downward towards the floor.

As a comment on the efficiency results for thermal comfort, we point out that the case of LOW ceiling panels is interesting: although they guarantee a small thermal stratification

(Figure 10) and provide the lowest operative temperature by far (Figure 11), they score a relatively high velocity at 1.7. m that is out of scale; see Table 6. Furthermore, Table 7 clearly proves that no correlation between surface temperature and operative temperature exists, as the HIGH ceiling panels have a lower temperature than the LOW panels. This confirms that when addressing thermal comfort, one needs to consider a whole combination of factors, including plumes generated by internal heat gains, and not only one parameter (e.g., the surface temperature).

Some limitations do exist for this study. First, the testing period was chosen between September and November to ensure less susceptibility to uncontrollable solar loads and external temperature swings. Moreover, as the internal heat gains used in the rooms were static loads, we did not address the systems' inertia nor control strategies.

The condensation risk was not assessed into detail either. The latent load of the rooms was minimal and primarily due to the dry supply air of the ventilation, which is usually more humid than during the tests. In real applications, avoiding condensation on the surfaces of the radiators, ceiling panels and the floor must be a priority. Condensation risk is determined by supply water temperature that was equal for all the devices.

The power output was highest for the FCU, which reached 1686 W or 54 W/m^2 even at the lowest fan setting and was also the only system to achieve more than 50 W/m^2. The other systems all provided close to 40 W/m^2; therefore, they are suitable to use with a relatively low cooling capacity by design and are accordingly not suitable to spaces where the cooling loads are larger than 50 W/m^2. As the temperature gradients are strongly related to energy efficiency (see, e.g., [30]), we also point out that in this respect our investigation is limited, as only one or two cooling output levels were measured. Adding measurements at different partial loads and considering additional boundary conditions such as ventilation supply temperature and flow rate as well as the internal and external surface temperatures in the room would provide a more comprehensive overview of the resulting temperature gradients.

5. Conclusions

In this paper, we addressed measurements of the cooling efficiency of radiant panels, fan-assisted radiators, fan coils, and underfloor cooling in terms of cooling power output and impact on thermal comfort. Six heating dummies were also placed within the room to mimic the internal gains of a typical office space. To assess thermal comfort, the change in temperature at different heights as well as the air velocities were observed together with the operative temperature.

Some significant stratification was observed for the underfloor cooling: for a seated occupant, the measured head-ankle temperature difference barely achieved category II for thermal comfort; for a standing occupant, this even worsened to category III. For the other systems, the stratification was milder, and gradients were generally of the order ~1.00 °C/m guaranteed category I. The operative temperature was evaluated as well: systems with larger radiant surfaces generally showed lower operative temperatures.

Air velocity magnitudes were the largest with the fan coil units, as expected. Even at the lowest fan speed setting, they only classified for thermal comfort category IV. All the other systems had lower velocities and achieved category I apart from the LOW ceiling panel, where the upward plume from the heating dummies or supply jets from ventilation valves probably prevailed.

Finally, a valuable result is that the cooling panels achieved a specific power of 36 W/m^2 per floor surface but 78 W/m^2 per radiant panel surface. Accordingly, they can be used even in rooms with a high cooling load if the panels are distributed as optimally as possible in the room ceiling. In summary, the most performing cooling devices for the studied 40 W/m^2 cooling application were the ceiling panels and fan-assisted radiators, followed by underfloor cooling having a limitation of stratification. Because of the strong jet, fan coil units cannot achieve thermal comfort within the whole occupied zone.

Although the investigation was quite thorough and articulated, it is affected by several limitations. As the testing occurred in September through November, a typical cooling season could not be addressed; static internal loads were used instead of more realistic dynamic heat gains; thus, control strategies were not assessed. Other possible refinements include investigating the condensation risk, testing devices with a larger cooling power, and adding enough measurement points to cover the measurement space entirely, thus representing the average gradient in the entire room. The results of this study are planned to be used for quantitative cooling emission efficiency analyses in further research.

Author Contributions: Conceptualization, K.-V.V., A.F. and J.K.; methodology, K.-V.V. and J.K.; software, K.-V.V.; validation, K.-V.V.; formal analysis, K.-V.V.; investigation, K.-V.V.; resources, J.K.; data curation, K.-V.V.; writing—original draft preparation, K.-V.V. and A.F.; writing—review and editing, K.-V.V. and A.F.; supervision, J.K.; project administration, J.K.; funding acquisition, J.K. All authors have read and agreed to the published version of the manuscript.

Funding: This work has been supported by the Estonian Ministry of Education and Research, European Regional Fund (grant 2014-2020.4.01.20-0289), by the European Commission through the H2020 project Finest Twins (grant No. 856602), the Estonian Centre of Excellence in Zero Energy and Resource Efficient Smart Buildings and Districts, ZEBE (grant 2014-2020.4.01.15-0016) funded by the European Regional Development Fund, the Estonian Research Council grant (PSG409), the Association of the European Heating Industry EHI member companies Orkli, Purmo Group, Zehnder Group and Vasco.

Data Availability Statement: Not applicable.

Conflicts of Interest: The authors declare no conflict of interest. The funders had no role in the design of the study; in the collection, analyses, or interpretation of data; in the writing of the manuscript, or in the decision to publish the results.

Nomenclature

K_p, K_i, K_d	Controller parameters (−)
u	Input signal (−)
ϕ	Cooling capacity (W)
G	Water flow (m^3/s)
c	Specific heat capacity of water (J/kg°C)
ρ	Water density (kg/m^3)
Δt	Difference between flow and return water temperatures (°C)
γ_i	Vertical air temperature difference for device *i* (°C)
γ_{TOT}	Total ceiling-floor gradient (°C)
t_z	Air temperature at height z (°C)
z	Height (m)
t_{op}	Operative temperature (°C)
ε	Surface emissivity (−)

References

1. Meehl, G.A.; Tebaldi, C. More Intense, More Frequent, and Longer Lasting Heat Waves in the 21st Century. *Science* **2004**, *305*, 994–997. [CrossRef] [PubMed]
2. Bienvenido-Huertas, D.; Rubio-Bellido, C.; Marín-García, D.; Canivell, J. Influence of the Representative Concentration Pathways (RCP) scenarios on the bioclimatic design strategies of the built environment. *Sustain. Cities Soc.* **2021**, *72*, 103042. [CrossRef]
3. Rogelj, J.; Popp, A.; Calvin, K.V.; Luderer, G.; Emmerling, J.; Gernaat, D.; Fujimori, S.; Strefler, J.; Hasegawa, T.; Marangoni, G.; et al. Scenarios towards limiting global mean temperature increase below 1.5 °C. *Nat. Clim. Change* **2018**, *8*, 325–332. [CrossRef]
4. Deroubaix, A.; Labuhn, I.; Camredon, M.; Gaubert, B.; Monerie, P.-A.; Popp, M.; Ramarohetra, J.; Ruprich-Robert, Y.; Silvers, L.G.; Siour, G. Large uncertainties in trends of energy demand for heating and cooling under climate change. *Nat. Commun.* **2021**, *12*, 5197. [CrossRef]
5. Hondula, D.M.; Balling, R.C.; Vanos, J.K.; Georgescu, M. Rising Temperatures, Human Health, and the Role of Adaptation. *Curr. Clim. Change Rep.* **2015**, *1*, 144–154. [CrossRef]

6. *CEN EN 15316-2*; Energy Performance of Buildings-Method for Calculation of System Energy Requirements and System Efficiencies-Part 2: Space Emission Systems (Heating and Cooling), Module M3-5, M4-5. European Committee for standardization: Bruxelles, Belgium, 2017.
7. Liu, H.; Wu, Y.; Li, B.; Cheng, Y.; Yao, R. Seasonal variation of thermal sensations in residential buildings in the Hot Summer and Cold Winter zone of China. *Energy Build.* **2017**, *140*, 9–18. [CrossRef]
8. Karmann, C.; Schiavon, S.; Bauman, F. Thermal comfort in buildings using radiant vs. all-air systems: A critical literature review. *Build. Environ.* **2017**, *111*, 123–131. [CrossRef]
9. Radzai, M.; Yaw, C.; Lim, C.; Koh, S.; Ahmad, N. Numerical Analysis on the Performance of a Radiant Cooling Panel with Serpentine-Based Design. *Energies* **2021**, *14*, 4744. [CrossRef]
10. Shin, M.-S.; Choi, J.-S.; Rhee, K.-N. Cooling Capacity and Energy Performance of Open-Type Ceiling Radiant Cooling Panel System with Air Circulators. *Energies* **2020**, *14*, 5. [CrossRef]
11. Ye, M.; Serageldin, A.A.; Radwan, A.; Sato, H.; Nagano, K. Thermal performance of ceiling radiant cooling panel with a segmented and concave surface: Laboratory analysis. *Appl. Therm. Eng.* **2021**, *196*, 117280. [CrossRef]
12. Park, S.-H.; Kim, D.-W.; Joe, G.-S.; Ryu, S.-R.; Yeo, M.-S.; Kim, K.-W. Establishing Boundary Conditions Considering Influence Factors of the Room Equipped with a Ceiling Radiant Cooling Panel. *Energies* **2020**, *13*, 1684. [CrossRef]
13. Erell, E.; Etzion, Y. Analysis and experimental verification of an improved cooling radiator. *Renew. Energy* **1999**, *16*, 700–703. [CrossRef]
14. Erell, E.; Etzion, Y. Radiative cooling of buildings with flat-plate solar collectors. *Build. Environ.* **2000**, *35*, 297–305. [CrossRef]
15. Myhren, J.H.; Holmberg, S. Summer time cooling with ventilation-radiators. In Proceedings of the Indoor Air Quality, Ventilation and Energy Conservation in Buildings, Sendai, Japan, 28–31 October 2007.
16. Zhao, K.; Liu, X.-H.; Jiang, Y. Application of radiant floor cooling in large space buildings—A review. *Renew. Sustain. Energy Rev.* **2016**, *55*, 1083–1096. [CrossRef]
17. Zhou, X.; Liu, Y.; Zhang, J.; Ye, L.; Luo, M. Radiant asymmetric thermal comfort evaluation for floor cooling system—A field study in office building. *Energy Build.* **2022**, *260*, 111917. [CrossRef]
18. Zhang, D.; Cai, N.; Cui, X.; Xia, X.; Shi, J.; Huang, X. Experimental investigation on model predictive control of radiant floor cooling combined with underfloor ventilation system. *Energy* **2019**, *176*, 23–33. [CrossRef]
19. Zeinelabdein, R.; Omer, S.; Gan, G. Critical review of latent heat storage systems for free cooling in buildings. *Renew. Sustain. Energy Rev.* **2018**, *82*, 2843–2868. [CrossRef]
20. Karakoyun, Y.; Acikgoz, O.; Yumurtacı, Z.; Dalkilic, A.S. An experimental investigation on heat transfer characteristics arising over an underfloor cooling system exposed to different radiant heating loads through walls. *Appl. Therm. Eng.* **2019**, *164*, 114517. [CrossRef]
21. Cen, C.; Jia, Y.; Liu, K.; Geng, R. Experimental comparison of thermal comfort during cooling with a fan coil system and radiant floor system at varying space heights. *Build. Environ.* **2018**, *141*, 71–79. [CrossRef]
22. Hu, B.; Wang, R.; Xiao, B.; He, L.; Zhang, W.; Zhang, S. Performance evaluation of different heating terminals used in air source heat pump system. *Int. J. Refrig.* **2019**, *98*, 274–282. [CrossRef]
23. Lin, B.; Liu, Y.; Wang, Z.; Pei, Z.; Davies, M. Measured energy use and indoor environment quality in green office buildings in China. *Energy Build.* **2016**, *129*, 9–18. [CrossRef]
24. Shan, X.; Zhou, J.; Chang, V.W.-C.; Yang, E.-H. Comparing mixing and displacement ventilation in tutorial rooms: Students' thermal comfort, sick building syndromes, and short-term performance. *Build. Environ.* **2016**, *102*, 128–137. [CrossRef]
25. Zhang, H.; Arens, E.; Zhai, Y. A review of the corrective power of personal comfort systems in non-neutral ambient environments. *Build. Environ.* **2015**, *91*, 15–41. [CrossRef]
26. Song, W.; Zhang, Z.; Chen, Z.; Wang, F.; Yang, B. Thermal comfort and energy performance of personal comfort systems (PCS): A systematic review and meta-analysis. *Energy Build.* **2021**, *256*, 111747. [CrossRef]
27. Tang, Y.; Yu, H.; Zhang, K.; Niu, K.; Mao, H.; Luo, M. Thermal comfort performance and energy-efficiency evaluation of six personal heating/cooling devices. *Build. Environ.* **2022**, *217*, 109069. [CrossRef]
28. Arghand, T.; Dalenbäck, J.-O.; Trüschel, A.; Javed, S. Some aspects of controlling radiant and convective cooling systems. *E3S Web Conf.* **2019**, *111*, 05008. [CrossRef]
29. NOBE. TTÜ Technology Testing Facility. Available online: https://nobe.ee/en/projektid/ttu-technology-testing-facility/ (accessed on 21 April 2022).
30. Maivel, M.; Ferrantelli, A.; Kurnitski, J. Experimental determination of radiator, underfloor and air heating emission losses due to stratification and operative temperature variations. *Energy Build.* **2018**, *166*, 220–228. [CrossRef]
31. Abel, E.; Voll, H.; Tark, T. *Hoonete Energiatarve ja Sisekliima*; OÜ Presshouse: Tallinn, Estonia, 2014.
32. *CEN EN 14240:2004*; Ventilation for Buildings-Chilled Ceilings-Testing and Rating. European Committee for Standardization: Bruxelles, Belgium, 2004.
33. *CEN EN 16798-1:2019*; Energy performance of buildings—Ventilation for buildings—Part 1: Indoor Environmental Input Parameters for Design and Assessment of Energy Performance of Buildings Addressing Indoor Air Quality, Thermal Environment, Lighting and Acoustics. European Committee for Standardization: Bruxelles, Belgium, 2019.